Article:
Yoon, JY, Zhang, H, Kim, YK et al. (2 more authors) (2019) A high-strength polyvinyl alcohol hydrogel membrane crosslinked by sulfosuccinic acid for strontium removal via filtration. Journal of Environmental Chemical Engineering, 7 (1). 102824. ISSN 2213-3437

https://doi.org/10.1016/j.jece.2018.102824

A High-strength Polyvinyl Alcohol Hydrogel Membrane Crosslinked by Sulfosuccinic Acid for Strontium Removal via Filtration

Ji Young Yoon[a,b,c], Huagui Zhang[b,d], Yun Kon Kim[a], David Harbottle[b,*], Jae W. Lee[a,*]

[a] Department of Chemical and Biomolecular Engineering, Korea Advanced Institute of Science and Technology (KAIST), Guseong-Dong, Yuseong-Gu, Daejeon, 34141, Republic of Korea

[b] School of Chemical and Process Engineering, University of Leeds, Leeds LS2 9JT, United Kingdom

[c] Drug and Disease Target Research Team, Division of Bioconvergence Analysis, Korea Basic Science Institute (KBSI), Cheongju 28119, Republic of Korea

[d] College of Chemistry and Materials Science, Fujian Key Laboratory of Polymer Science, Fujian Normal University, Fuzhou 350007, China

KEYWORDS: Strontium removal, Polyvinyl alcohol, Sulfosuccinic acid, Mechanical stability, Membrane filtration

Abstract

This study considered the removal of strontium (Sr^{2+}) from contaminated water using a filtration membrane that exhibits good mechanical strength, high adsorption capacity, and the ability to be regenerated and reused. Polyvinyl alcohol hydrogel membranes were prepared by crosslinking with sulfosuccinic acid in different ratios (2.5, 5, 10 and 20 mol% relative to the PVA monomer), named as PSA2.5, PSA5, PSA10 and PSA20. All PSA membranes showed good Sr^{2+} adsorption over a wide pH range (pH 2-12), and maintained rapid removal kinetics (> 95 % Sr^{2+} recovered from 5 ppm Sr^{2+} within 4 h). Furthermore, the Sr^{2+} adsorption capacities of PSA2.5, PSA5, PSA10 and PSA20 were 27.6, 45.8, 56.3, and 55.3 mg/g, respectively, based on the Langmuir adsorption isotherm. From the four PSA membranes, PSA5 was selected for further filtration studies due to its favorable mechanical and adsorption properties. When filtering 5 ppm Sr^{2+} and 250 ppm Ca^{2+}, corresponding to the Ca^{2+} concentration in the wastewater at the Fukushima nuclear plant, 87% Sr^{2+} was removed using the PSA5 membrane following multiple cycles of regeneration and reuse. Moreover, the tensile strength of the PSA5 membrane remained high (> 100 MPa) following five consecutive uses.

1. Introduction

After the incident at the Fukushima Nuclear Power Plant (Japan) in March 2011, a significant release of radionuclides into nearby seawater/groundwater [1] has led to significant environmental radioactive contamination, with radionuclides ^{90}Sr and ^{137}Cs of particular concern due to their high fission yields and substantial half-lives (approximately 30years) [1, 2]. The reported ^{90}Sr levels (400 $kBqm^{-3}$) were higher than the pre-incident level (1.2 Bqm^{-3}) and underlined the need to recover ^{90}Sr from the environment [3, 4]. Furthermore, ^{90}Sr can accumulate and cause serious health issues due to strong similarities to Ca^{2+}, i.e. hydration size and ionic charge [5]. Removal of ^{90}Sr from wastewater is therefore essential, along with other radionuclides which has been the focus of additional removal studies [3, 6, 7].

Several methods have already been considered to recover strontium from wastewater including solvent extraction [8], chemical precipitation [9], coagulation [10], and electrodialysis [11]. However, these methods can produce large volumes of secondary wastes [12], hence, adsorption methods are particularly attractive due to their simplicity, small waste volume and high adsorption capacity [13]. Typical adsorbents such as metal oxides and crown ethers require very stringent synthesis conditions (e.g. complex, multi-step synthesis routes) and the material cost can sometimes be prohibitive. The use of natural adsorbents such as zeolites and clays are of interest but often the materials have to be chemically treated to produce desirable adsorption selectivity [14-17]. Therefore, a simple synthesis route utilizing lower cost materials is clearly desirable for practical applications.

Polymers such as chitosan, alginate, carboxymethyl cellulose, polyacrylonitrile and polyvinyl alcohol have been used to prepare adsorbents for the removal of hazardous metal ions from wastewater [18-22]. Among those polymers, polyvinyl alcohol (PVA) is particularly interesting from an economic and material (biodegradable) perspective, being widely utilized in drug delivery systems [23], methanol fuel cells [24], and metal removal [25]. PVA-based adsorbents have been prepared via various synthesis routes including chemical crosslinking reaction and freeze-thaw [21, 26]. The removal of radionuclides/heavy metal ions such as cesium [26], copper [27], and nickel [28] has been demonstrated, with flexibility to modify the adsorbent

form for column applications (micron-sized beads) [29], and responsive recovery from wastewater systems (immobilized magnetic particles) [26]. To be considered useful, the material must exhibit high removal efficiency of the targeted ion, maintain good adsorption performance in the presence of many competing ions such as sodium, potassium and calcium (prevalent ions in seawater [30]), and remain mechanically stable for long-term use/re-use.

A PVA-based membrane crosslinked with sulfosuccinic acid (SSA) has been considered in the current study. Though sulfonate [31], polyethyleneimine [32], chitosan [33] and acrylic acid [34] have been used as crosslinkers of PVA, the main applications of these membranes have been for methanol fuel cell technology and the removal of heavy metals such as Cu^{2+}, Pb^{2+} and Zn^{2+}. From a previous study [24], a sulfonate pendent group was bonded to PVA and then crosslinked (using a secondary additive) to improve mechanical stability of the membrane via a two-step method. In the current study, SSA was chosen to crosslink PVA and act as an ion exchange donor site, SO_3H. By crosslinking SSA to PVA in a single step, the mechanical stability of PVA could be enhanced along with the adsorption capacity for Sr^{2+} via the numerous ion exchange sites (SO_3H).

2. Materials and Methods

2.1. Materials

Polyvinyl alcohol (PVA, Mw 89,000 – 98,000 g/mol, 99% hydrolyzed) and sulfosuccinic acid (SSA, 70% w/v in aqueous solution) were purchased from Sigma Aldrich. For the batch adsorption tests, chloride salts were used and purchased from Sigma Aldrich (KCl, NaCl, $CaCl_2$ and $MgCl_2 \cdot 6H_2O$) and Fisher Scientific ($SrCl_2 \cdot 6H_2O$). Hydrochloric acid solution (HCl, 37%) was used to regenerate the adsorbent and was purchased from Sigma Aldrich. Milli-Q water with resistivity of 18.2 MΩ·cm was used throughout the study. Standard solution of 1000 ppm Sr^{2+} (Sigma Aldrich) was used to produce a calibration curve for analysis by inductively coupled plasma-mass spectrometry (ICP-MS).

2.2. Synthesis of PVA membrane crosslinked by SSA (PSA membrane)

PVA polymer was slowly dissolved in Milli-Q water to a concentration of 10% (w/v) by gentle stirring for 3 h at 90 °C until the solution appeared transparent. The solution was then cooled

down to room temperature. SSA solution was added dropwise into the PVA solution at varying SSA concentrations (2.5, 5, 10 and 20 mol%) relative to the PVA monomer. Each PVA-SSA solution was stirred at room temperature for 24 h before being poured into separate Teflon moulds. The solutions were dried at ambient temperature for 2 days before heating at 110 ℃ for 1 h to promote crosslinking between PVA and SSA. The as-prepared PVA membranes crosslinked with 2.5, 5, 10 and 20 mol% SSA were named as PSA2.5, PSA5, PSA10 and PSA20, respectively. For the control sample, a PVA membrane in the absence of SSA was also synthesized following the same procedure.

2.3. Membrane characterization

The Fourier transformed infrared (FT-IR) spectra of the PSA membranes were measured using a Nicolet is10 FT-IR Spectrometer (Thermo Fisher Scientific, USA) in the range of 4000-600 cm^{-1}. An X-ray diffractometer (XRD) with a CuKα beam was used to determine the physical structure of the membranes using a Philips X'pert (Philips, USA), with a rotating anode X-ray source operating at 40 kV and 40 mA. Using a Shimadzu TGA-50 (Shimadzu, Japan), thermogravimetric analysis (TGA) was completed on all PSA membranes up to 600 ℃ at a heating rate of 10 ℃ min^{-1} in a nitrogen atmosphere. Cryo-SEM with a PP3010T Cryo-SEM preparation system (Quorum Technologies, UK) was used to study the membrane morphology after swelling each membrane in Milli-Q water.

The mechanical properties of the PSA membranes were studied using a Titan tensile strength tester (James Heal co., UK). The PSA membranes were cut to size (10 mm width and 40 mm length) and the thickness measured to be in the range of 100-300 µm. Only test samples with no visual defects were considered to ensure good reproducibility. The rate of sample extension was 100 mm/min and tests were carried out at room temperature. All mechanical properties including the Young's modulus, tensile strength and critical strain at yielding were an average of three repeat measurements.

Water absorption by the PSA membranes was estimated from the mass change before and after immersing the membranes in Milli-Q water or 200 ppm Sr^{2+} solution at 25 ℃ for 24 h. All membranes were dried under vacuum at 50 ℃ for 24 h to remove any bound water and then

immersed in water for 24 h before being removed and gently touched to filter paper to absorb any surface water. The water absorption (%) is given by

$$\text{Water absorption (\%)} = \frac{w_s - w_d}{w_d} \times 100 \quad (1)$$

where w_d is the dry sample weight and w_s is the weight after water absorption.

2.4. Batch adsorption of Sr^{2+}

Batch adsorption of Sr^{2+} was measured as a function of solution pH, membrane-solution contact time, adsorbent amount and in the presence of competitive ions. The Sr^{2+} concentration in the simulated water remained fixed at 5 ppm. All Sr^{2+} batch adsorption studies were conducted using a mechanical orbital shaker operated at 150 rpm for 24 h at room temperature. For the pH-dependent study, the solution pH was adjusted between pH 2 and 12 by the dropwise addition of either 0.1 M NaOH or 0.1 M HCl.

To measure the adsorption kinetics, small volumes (0.5 % of the total solution volume) were removed at pre-determined time intervals. For the adsorbent amount study, the adsorbent content was varied from 0.05 to 1 g/L in the simulated water. To evaluate the performance of the PSA membrane in the presence of competitive ions, the Sr^{2+} concentration was fixed at 5 ppm and the concentrations of K^+, Na^+, Ca^{2+} and Mg^{2+} were varied from 0 to 1000 ppm. The amount of Sr^{2+} removed, Q_t (mg g^{-1}), and the removal efficiency, RE (%), were calculated by [35]

$$Q_t = (C_0 - C_t) \times \frac{v}{m} \quad (2)$$

$$RE = \frac{C_0 - C_t}{C_0} \times 100 \quad (3)$$

where C_0 (mg L^{-1}) is the initial Sr^{2+}concentration, C_t (mg L^{-1}) the Sr^{2+} concentration after time t (min), V(L) is the solution volume, and m (g) the adsorbent mass.

Adsorption isotherms for each PSA membrane were determined over a range of Sr^{2+} concentrations, 5 to 200 ppm. Sr^{2+} concentration after adsorption was measured by ICP-MS (Elan DRC-e, PerkinElmer, USA). For solutions with a high Sr^{2+} concentration, the sampled

volume was diluted using Milli-Q water to ensure the concentration was in the range for the ICP-MS measurement (< 10 ppm).

2.5. Membrane filtration

A continuous flow filtration system (All pond solutions, UK) was used to study Sr^{2+} adsorption by a filtration cartridge loaded with 4 g PSA membrane. 2 L of the simulated water, 5 ppm Sr^{2+} and 250 ppm Ca^{2+}, was recirculated through the PSA membrane at a flow rate of 400 L/h. Each adsorption test was conducted for 6 h with the Sr^{2+} removal determined after each cycle. Following each test, the PSA membrane was regenerated by soaking in 0.3 M HCl solution for 3 h and washed thoroughly with Milli-Q water prior to reuse. The PSA membrane was regenerated and reused five times. After each cycle, a small amount of the simulated water was removed and analyzed using ICP-MS to determine the remaining Sr^{2+} concentration.

3. Results and Discussion

3.1. Characterization of PSA membrane

3.1.1. Chemical structure

PSA membranes were prepared by a crosslinking reaction between hydroxyl (-OH) and carboxyl (-COOH) groups of PVA and SSA, respectively, see Figure 1(A). The PSA membrane turned black after the crosslinking reaction as shown in Figure 1(B). Figure 1(C) identifies the chemical bonding and functional groups of the crosslinked PSA compared to pure PVA. All PSA membranes showed the C=O stretch and the symmetry vibration of the sulfonic group ($-SO_3^-$) of SSA at around 1700-1750 cm^{-1} and 1031-1056 cm^{-1}, respectively, with an increase of peak intensities for increasing SSA content. Furthermore, the peak at 1211-1224 cm^{-1} corresponds to ester bonding (C-O-C) and symmetric stretching of $-SO_3^-$ [31], formed by the crosslinking reaction of PVA and SSA. The peak intensity of the O-H stretching vibration at 3000-3500 cm^{-1} was weakened in the PSA membranes as compared to the pure PVA membrane.

3.1.2. Physical characterization

The crystallinity and morphology of the PSA membranes were determined by X-ray diffraction and cryo-SEM as shown in Figures 2(A) and (B). As seen in Figure 2(A), pure PVA showed a strong sharp diffraction peak at 2theta = 19.5° and a weaker peak at 2theta = 22.6°. The main

crystalline peak at 2theta = 19.5° reveals the characteristic (101) plane of semi-crystalline PVA [36]. Typically, as the crosslinking ratio of a copolymer network is increased the network becomes more amorphous [37]. Figure 2(A) shows a decrease in the crystalline peak intensity (characteristic peak of pure PVA, 2θ = 19.5°, 22.6° [36]) of the PSA membrane with increasing SSA content, and peak broadening with a shoulder appearing at 2θ = 40° confirming the loss of crystallinity. The morphology of swelled PSA membranes was observed using cryo-SEM, see Figure 2(B). PSA20 revealed an ordered mesoporous structure that was not readily observed in the other membranes. The ordered mesoporous structure can be explained by significant hydrogen bonding between pendant groups such as sulfonic and hydroxyl groups [38].

3.1.3. Thermal stability

Thermal decomposition of the PSA membranes with increasing SSA content was studied using TGA, see Figure 3. The PVA membrane showed a 5 wt% reduction of mass over the temperature range 25 to 170 °C which can be attributed to the loss of adsorbed water. At temperatures above 250 °C, removal of hydroxyl groups and main chain (-CH_2) decomposition of PVA occurred. All PSA membranes exhibited three stages of thermal decomposition, tentatively defined by the dash lines in Figure 3. The first stage corresponds to the temperature range of 25 to 170 °C where mass loss is attributed to the removal of bound water from the PSA membrane. The second stage corresponds to mass loss at intermediate temperatures ~220 - 304 °C resulting from the decomposition of OH, SO_2, SO, SO_3H and breakage of the ester bonds (CO-O-), with an increase in mass loss corresponding to the increased SSA content [31]. The mass loss in the final stage at much higher temperatures ~460 - 525 °C is a result of CH_2 decomposition of PVA.

Furthermore, all PSA membranes exhibited greater thermal stability than the pure PVA membrane with more thermal energy required to break the crosslinked bond [39]. Therefore, by increasing the crosslinking density of the PSA membrane, more PSA membrane remained after thermal decomposition. Figure 3 shows that the remaining mass (at 600 °C) of PSA membrane containing 2.5, 5, 10 and 20 mol% SSA was 22.5 %, 24.0 %, 33.0 % and 29.8 % of the initial mass, respectively, with only 4.9 % of the pure PVA membrane remaining.

Interestingly, the remaining mass of PSA20 was lower than PSA10, even though the SSA content was higher. Above a certain SSA content, the crosslinking density within the PSA membrane decreased. For PSA20, any un-reacted SSA within the membrane will disrupt the crosslink bond (C-O-C) between PVA and SSA, which has been verified by the porous structure of the PSA membrane, see the cryo-SEM in Figure 2(B). Therefore, if the crosslinked ratio of PSA20 is less than PSA10 as a result of any un-reacted SSA, then the membrane residue remaining will be less.

3.1.4. Mechanical strength

The mechanical strength of the formed PSA membrane is an important property when considering the application. Tensile stress-strain curves of PVA and PSA membranes are shown in Figure 4(A) and the mechanical properties summarized in Table 1. Based on the yielding of PSA and PVA membranes, the mechanical strength of the membrane was shown to be sensitive to the SSA content. Compared to pure PVA (78.4 MPa), the yield strengths of PSA2.5 and PSA5 increased by 63 % (from 78.4 to 128.1 MPa) and 85 % (from 78.4 to 145.2 MPa), respectively, while PSA10 and PSA20 decreased by 43 % (from 78.4 to 45.2 MPa) and 97 % (78.4 to 2.0 MPa), respectively. The results show that the yield strength of the PSA membrane decreases when the SSA content is greater than 5 mol% (Figure 4(B). All PSA membranes have some bound water interacting with sulfonic group via hydrogen bonding, even following sample drying (see Figure S1). The higher the SSA content, the more water retained by the PSA membrane. As such, bound water can act as a plasticizer of the membrane, weakening the mechanical stability of the membrane [40]. While SSA acts as a crosslinker, enhanced mechanical stability of PSA in the presence of 2.5 and 5 mol% SSA, at a higher crosslinking density (PSA10 and PSA20), the bound water acted as a plasticizer interacting with sulfonic groups and reducing the membrane mechanical stability.

Moreover, the membrane elongation at break was similar for all PSA membranes except PSA20. The PSA20 membrane exhibited the largest elongation at break (45.5 %) as well as exhibiting the lowest tensile strength amongst all membranes. Based on our previous observations, the PSA20 membrane was more porous, with the mesoporous structure resulting in a more ductile response [41].

3.2. Batch adsorption of Sr^{2+} by PSA membranes

3.2.1. Effect of pH

The effect of pH on Sr^{2+} removal by the PSA membranes was evaluated in a system of 5 ppm Sr^{2+} solution. Figure 5(A) shows no Sr^{2+} removal by the PVA membrane, while all PSA membranes removed 99 % Sr^{2+} over the pH range 3 to 10. Even in the most unfavorable condition, pH 1.5, all PSA membranes showed good Sr^{2+} removal efficiency with recoveries greater than 60 %. At pH 1.5, an excess of H^+ competes with Sr^{2+} for the available ion exchange sites (SO_3^-) in the PSA membrane. With a decrease in the SSA ratio, the adsorption site density decreased, hence the effect of reduced Sr^{2+} adsorption becomes more significant. Furthermore, although the Sr^{2+} removal efficiency (%) reduced slightly at pH 12, the recovery was still greater than 92 %. An excess of OH^- in the Sr^{2+} solution can decrease ion exchange due to the formation of hydroxyl complexes of Sr^{2+} [42, 43]. Overall, the PSA membranes demonstrated good to excellent Sr^{2+} removal over a wide pH range, making them suitable for application in harsh processing environments. Following the pH stability testing, all further batch adsorption tests were completed at pH 6.

3.2.2. Effect of adsorbent amount

To determine the optimal adsorbent amount, the adsorbent (PSA membrane) content was varied from 0.01 to 1 g/L in a 5 ppm Sr^{2+} solution. Figure 5(B) shows that Sr^{2+} removal efficiencies for all PSA membranes increased with the increasing adsorbent content, while PVA showed negligible Sr^{2+} adsorption under all conditions tested. PSA2.5 removed 99 % of the 5 ppm Sr^{2+} for an adsorbent amount $\geq$ 0.5 g/L, with all other PSA membranes achieving the same level of removal at 0.25 g/L. For further batch adsorption testing, 1 g/L PSA membrane was used.

3.2.3. Effect of adsorbent-solution contact time

The adsorption kinetics of Sr^{2+} by the PSA membranes were evaluated as a function of adsorbent-solution contact time. All PSA membranes showed rapid Sr^{2+} adsorption within 4 h with a maximum removal efficiency of 99% achieved in 5 h as shown in Figure 5(C). As such, all further adsorption batch tests were completed for 6 h.

Furthermore, the experimental data were fitted to both pseudo-first order and pseudo-second order equations [44], Eq. (4) and Eq. (5), respectively, to better understand the sorption mechanism, with the fitting parameters summarized in Table 2 (refer to Figure 5(D)).

Pseudo-first order equation

$$\ln(Q_e - Q_t) = lnQ_e - k_1 t \quad (4)$$

Pseudo-second order equation

$$\frac{t}{Q_t} = \frac{1}{k_2 Q_e^2} + \frac{t}{Q_e} \quad (5)$$

where Q_e and Q_t are the sorption capacities (mg/g) at equilibrium and at time t, respectively; k_1 and k_2 are the pseudo-first and -second order rate constants (L/min), respectively.

Comparing the fitting parameters for the two kinetic models (Table 2), it can be seen that the pseudo-second order model provides much better agreement to the measured Sr^{2+} adsorption kinetics for all PSA membranes, as shown by the linear plot in Figure 5(D) with the coefficients of determination greater than 0.99. As such, Sr^{2+} adsorption by all PSA membranes likely follows a chemisorption process such as ion exchange rather than physisorption [45, 46].

3.2.4. Sr^{2+} adsorption isotherm

Each PSA membrane has a finite capacity for Sr^{2+} as shown by the adsorption isotherms in Figure 6. The Langmuir (Eq. 6) and Freundlich (Eq. 7) equations were used to fit the experimental data as shown in Figures 6(A) and (B), respectively, with the fitting parameters summarized in Table 3.

The Langmuir isotherm is given by

$$Q_e = \frac{Q_m b C_e}{(1 + bC_e)} \quad (6)$$

where Q_e is the amount of Sr^{2+} adsorbed (mg/g) at equilibrium, C_e the Sr^{2+} concentration in solution at equilibrium (mg/L), Q_m and b are fitting parameters which describe the maximum adsorption capacity (mg/g) and the affinity coefficient (L/mg), respectively.

The Freundlich isotherm is given by

$$Q_e = K_f C_e^{1/n} \quad (7)$$

where K_f is the Freundlich constant relating to Sr^{2+} adsorption capacity (mg/g), and 1/n is an indication of adsorption intensity or surface heterogeneity.

The Langmuir adsorption isotherm describes monolayer coverage of the surface with all adsorption sites energetically similar, while the Freundlich isotherm describes a heterogeneous multilayered surface, with non-uniform distribution of adsorption affinities over the heterogeneous surface [22]. All PSA membranes showed better agreement with the Langmuir isotherm with $R^2 > 0.95$ (Table 3). This indicates that adsorption was mainly dominated by the homogeneous ion exchange site at sulfonic groups (-SO_3H) in the PSA membranes. From the Langmuir fitting parameters revealed in Table 3, Sr^{2+} adsorption capacities of PSA2.5, PSA5, PSA10 and PSA20 were 27.6, 45.8, 56.3 and 55.3 mg/g, respectively.

The ion-exchange mechanism between Sr^{2+} and the PSA membrane is proposed as followed [47]:

$$2SO_3H + Sr^{2+} \rightarrow (SO_3)_2^- Sr^{2+} + 2H^+$$

where one divalent Sr^{2+} ion is exchanged with two protons from the sulfonic group [48]. The theoretical number of ion exchange sites (SO_3H) within each PSA membrane and hence the Sr^{2+} adsorption capacity has been considered in Figure 7(A). As the SSA content in the PSA membrane increases, then the capacity of the PSA membrane to adsorb Sr^{2+} should also increase. However, when the experimental data is compared to the theoretical capacity (Figure 7(A), Table S1), a plateau in the amount of Sr^{2+} adsorbed was observed for PSA10 and PSA20, and the theory overpredicts the measured data. It appears that the amount of Sr^{2+} adsorbed does not increase proportionally with increasing ion exchange sites in the PSA membrane. Such behavior also corresponds with the Sr^{2+} adsorption affinity represented by the Langmuir fitting parameter, b, as shown in Table 3, with PSA2.5 and PSA5 exhibiting a higher adsorption affinity for Sr^{2+} compared to PSA10 and PSA20. As such, other parameters appear to influence the adsorption capacity of the PSA membranes.

Hydration of the PSA membranes was measured with the water uptake calculated using Eq. 1. Water uptake by the PSA membranes in 200 ppm Sr^{2+} solution was lower than in Milli-Q water, see Table 3 (refer to Figure S2(A)). When the affinity of the counter-ion for the sulfonic acid

group increases, the bond polarity decreases as the bond becomes more covalent, therefore the water uptake generally decreases [37, 49]. The high affinity of Sr^{2+} for the sulfonic acid group in 200 ppm Sr^{2+} solution may contribute to the lower water uptake. The degree of water uptake by PSA membranes of increasing SSA content and their associated adsorption capacities for Sr^{2+} are in excellent agreement, see Figure 7(B) and Figure S2(B). Based on these findings, the observed plateau in Sr^{2+} adsorption capacity for PSA10 and PSA20 can be attributed to the reduced water uptake.

3.2.5. Effect of competing ions

To simulate nuclear plant conditions, Sr^{2+} adsorption was evaluated in the presence of competing cations such as K^+, Na^+, Ca^{2+}, and Mg^{2+} (Figure 8). Divalent ions significantly inhibited Sr^{2+} adsorption more than monovalent ions (K^+, Na^+), since adsorption is strongly influenced by the charge density and size of the hydrated ion. In particular, Ca^{2+} and Sr^{2+} have equivalent hydrated ion radii of 4.12 Å [2], thus Ca^{2+} can strongly compete for the SO_3H ion exchange sites. The negative effect of competitive ions can be mitigated by increasing the amount (g) of adsorbent per L solution. At 1 g/L and 250 ppm Ca^{2+}, the Sr^{2+} removal efficiency (initial Sr^{2+} concentration 5 ppm) was less than 15 % for all PSA membranes. However, when the amount of adsorbent was increased to 15 g/L, the Sr^{2+} removal efficiencies of PSA2.5, 5, 10 and 20 were improved to 58.9 %, 91.4 %, 94.1 % and 87.2 %, respectively, see Figure S3.

3.3. Continuous flow membrane filtration

The PSA5 membrane showed the best mechanical stability and reasonable Sr^{2+} adsorption capacity compared to other adsorbents (Table 4), hence the PSA5 membrane was chosen for further testing using the continuous flow membrane filtration system (see Figure 9A and Figure S4). A cut-to-size PSA5 membrane was inserted into the water purification system and the amount of Sr^{2+} removed (initial Sr^{2+} concentration = 5 ppm) in the presence of 250 ppm Ca^{2+} was measured following 6h of cycling the simulated water through the membrane at a rate of 400 L/h. Following each test, the membrane was removed and regenerated following the method described and then re-tested against the same simulated water, i.e. the Sr^{2+} and Ca^{2+} concentrations were not readjusted to the initial concentrations. After the first test, 47 ± 0.5 % of the 5 ppm Sr^{2+} was recovered with 87 ± 0.02 % of the initial Sr^{2+} recovered after the 5^{th} test

and four regenerations of the PSA membrane, see Figure 9(B).

Furthermore, the mechanical properties of the PSA5 membrane were evaluated following the 5 filtration tests, since ion adsorption and exposure to a strong ionic solution can deteriorate the mechanical integrity of adsorbents [30]. Following the 5 filtration tests, the PSA5 membrane exhibited good tensile strength (Figure 9(C)) and was comparable to the freshly prepared membrane, with the fracture tensile strength of the PSA5 membrane before and after use equal to 145 MPa and 123 MPa, respectively, which for a membrane is considered to be high strength when the tensile strength is in excess of 100 MPa [50].

4. Conclusion

The current study developed a high-strength PSA membrane for Sr^{2+} removal via filtration. The desirable properties of the PSA membrane including good mechanical stability, excellent Sr^{2+} selectivity and adsorption capacity can be attributed to the inclusion of SSA which acts to crosslink the PVA and provides ion adsorption sites for Sr^{2+}. Among all PSA membranes synthesized, PSA5 revealed the best mechanical properties and reasonable Sr^{2+} adsorption capacity. Sr^{2+} adsorption increased with increasing PVA-SSA crosslinking, although unreacted SSA at high SSA concentrations reduced the crosslinking density of PSA20 leading to the formation of a mesoporous membrane structure which did not strongly hydrate leading to a plateau (same as PSA10) in the performance of Sr^{2+} adsorption. Using the PSA5 membrane in a continuous flow filtration system, 87 % Sr^{2+} was removed from simulated water containing 250 ppm Ca^{2+} after five test cycles and four regenerations of the membrane using 0.3M HCl. The study has demonstrated the method to synthesize PSA membranes to remove Sr^{2+} from a range of complex aqueous environments. Based on its promising Sr^{2+} adsorption properties, the PSA membrane is a suitable candidate for further modification and inclusion of hexacyanoferrate to promote dual (Sr^{2+} and Cs^{+}) adsorption. This is currently part of an ongoing study which is showing promise.

Acknowledgement

The authors are grateful for the financial support from the UK-Republic of Korea Joint Research Program. J. W. Lee acknowledges the NRF grant (NRF-2015M2A7A1000219)

funded by the Ministry of Science, ICT, and Future Planning. D. Harbottle acknowledges the financial support of the Engineering and Physical Sciences Research Council grant number EP/M026426/1.

References

[1] P.P. Povinec, K. Hirose, M. Aoyama, Radiostrontium in the western North Pacific: characteristics, behavior, and the Fukushima impact, Environmental science & technology 46 (2012) 10356-10363.

[2] W. Mu, Q. Yu, X. Li, H. Wei, Y. Jian, Efficient removal of Cs^{+} and Sr^{2+} from aqueous solution using hierarchically structured hexagonal tungsten trioxide coated Fe_3O_4, Chemical Engineering Journal 319 (2017) 170-178.

[3] N. Casacuberta, Masqué, P., Garcia-Orellana, J., Garcia-Tenorio, R., and Buesseler, K. O., 90Sr and 89Sr in seawater off Japan as a consequence of the Fukushima Dai-ichi nuclear accident, Biogeosciences 10 (2013) 3649-3659.

[4] T.M. Paul Sylvester, Jesse Jensen, Radioactive liquid waste treatment at Fukushima Daiichi, Journal of Chemical Technology and Biotechnology 88 (2013) 1592-1596.

[5] S.K. Sahoo, N. Kavasi, A. Sorimachi, H. Arae, S. Tokonami, J.W. Mietelski, E. Lokas, S. Yoshida, Strontium-90 activity concentration in soil samples from the exclusion zone of the Fukushima daiichi nuclear power plant, Scientific reports 6 (2016) 23925.

[6] M.R. Awual, T. Yaita, Y. Miyazaki, D. Matsumura, H. Shiwaku, T. Taguchi, A Reliable Hybrid Adsorbent for Efficient Radioactive Cesium Accumulation from Contaminated Wastewater, Scientific reports 6 (2016) 19937.

[7] D. Yamaguchi, K. Furukawa, M. Takasuga, K. Watanabe, A Magnetic Carbon Sorbent for Radioactive Material from the Fukushima Nuclear Accident, Scientific reports 4 (2014) 6053.

[8] C. Xu, J. Wang, J. Chen, Solvent Extraction of Strontium and Cesium: A Review of Recent Progress, Solvent Extraction and Ion Exchange 30 (2012) 623-650.

[9] T. Zhang, K. Gregory, R.W. Hammack, R.D. Vidic, Co-precipitation of radium with barium and strontium sulfate and its impact on the fate of radium during treatment of produced water from unconventional gas extraction, Environmental science & technology 48 (2014) 4596-4603.

[10] P.S. Bull, J.V. Evans, R.J. Knight, Removal of radioactive strontium from water by

coagulation–flocculation with ferric hydroxide, Journal of Applied Chemistry and Biotechnology 25 (1975) 801-807.
[11] M.S. Gasser, H.G. Nowier, Separation of strontium and cadmium ions from nitrate medium by ion-exchange membrane in an electrodialysis system, Journal of Chemical Technology & Biotechnology 79 (2004) 97-102.
[12] F. Fu, Q. Wang, Removal of heavy metal ions from wastewaters: a review, Journal of environmental management 92 (2011) 407-418.
[13] M.R. Awual, T. Yaita, T. Taguchi, H. Shiwaku, S. Suzuki, Y. Okamoto, Selective cesium removal from radioactive liquid waste by crown ether immobilized new class conjugate adsorbent, Journal of hazardous materials 278 (2014) 227-235.
[14] M.R. Awual, Ring size dependent crown ether based mesoporous adsorbent for high cesium adsorption from wastewater, Chem. Eng. J. 303 (2016) 539-546.
[15] M.R. Awual, S. Suzuki, T. Taguchi, H. Shiwaku, Y. Okamoto, T. Yaita, Radioactive cesium removal from nuclear wastewater by novel inorganic and conjugate adsorbents, Chem. Eng. J. 242 (2014) 127-135.
[16] H.Y. Zhu, Y.Q. Fu, R. Jiang, J.H. Jiang, L. Xiao, G.M. Zeng, S.L. Zhao, Y. Wang, Adsorption removal of congo red onto magnetic cellulose/Fe3O4/activated carbon composite: Equilibrium, kinetic and thermodynamic studies, Chem. Eng. J. 173 (2011) 494-502.
[17] H. Zhang, Y.K. Kim, T.N. Hunter, A.P. Brown, J.W. Lee, D. Harbottle, Organically modified clay with potassium copper hexacyanoferrate for enhanced Cs^{+} adsorption capacity and selective recovery by flotation, Journal of Materials Chemistry A 5 (2017) 15130-15143.
[18] U. Habiba, A.M. Afifi, A. Salleh, B.C. Ang, Chitosan/(polyvinyl alcohol)/zeolite electrospun composite nanofibrous membrane for adsorption of Cr^{6+}, Fe^{3+} and Ni^{2+}, Journal of hazardous materials 322 (2017) 182-194.
[19] H.J. Hong, H.S. Jeong, B.G. Kim, J. Hong, I.S. Park, T. Ryu, K.S. Chung, H. Kim, J. Ryu, Highly stable and magnetically separable alginate/Fe3O4 composite for the removal of strontium (Sr) from seawater, Chemosphere 165 (2016) 231-238.
[20] Y. Kim, Y.K. Kim, S. Kim, D. Harbottle, J.W. Lee, Nanostructured potassium copper hexacyanoferrate-cellulose hydrogel for selective and rapid cesium adsorption, Chem. Eng. J. 313 (2017) 1042-1050.
[21] Y.K. Kim, Y. Kim, S. Kim, D. Harbottle, J.W. Lee, Solvent-assisted synthesis of potassium

copper hexacyanoferrate embedded 3D-interconnected porous hydrogel for highly selective and rapid cesium ion removal, Journal of Environmental Chemical Engineering 5 (2017) 975-986.

[22] A. Nilchi, R. Saberi, M. Moradi, H. Azizpour, R. Zarghami, Adsorption of cesium on copper hexacyanoferrate–PAN composite ion exchanger from aqueous solution, Chem. Eng. J. 172 (2011) 572-580.

[23] W. Chen, K. Achazi, B. Schade, R. Haag, Charge-conversional and reduction-sensitive poly(vinyl alcohol) nanogels for enhanced cell uptake and efficient intracellular doxorubicin release, Journal of Controlled Release 205 (2015) 15-24.

[24] N. Seeponkai, J. Wootthikanokkhan, Proton conductivity and methanol permeability of sulfonated poly(vinyl alcohol) membranes modified by using sulfoacetic acid and poly(acrylic acid), Journal of Applied Polymer Science 105 (2007) 838-845.

[25] A. Idris, Z. Majidnia, K.S.b. Nor Kamarudin, Photocatalyst treatment for lead(II) using titanium oxide nanoparticles embedded in PVA-alginate beads, Desalination and Water Treatment 57 (2016) 5035-5044.

[26] Y.K. Kim, T. Kim, Y. Kim, D. Harbottle, J.W. Lee, Highly effective Cs^+ removal by turbidity-free potassium copper hexacyanoferrate-immobilized magnetic hydrogels, Journal of hazardous materials 340 (2017) 130-139.

[27] W.S. NgahAKamariY.JKoay, Equilibrium and kinetics studies of adsorption of copper (II) on chitosan and chitosan/PVA beads, International journal of biological macromolecules 34 (2004) 155-161.

[28] M. Irani, A.R. Keshtkar, M.A. Mousavian, Removal of Cd(II) and Ni(II) from aqueous solution by PVA/TEOS/TMPTMS hybrid membrane, Chemical Engineering Journal 175 (2011) 251-259.

[29] H. Yang, H. Li, J. Zhai, L. Sun, Y. Zhao, H. Yu, Magnetic prussian blue/graphene oxide nanocomposites caged in calcium alginate microbeads for elimination of cesium ions from water and soil, Chemical Engineering Journal 246 (2014) 10-19.

[30] S.-C. Jang, S.-M. Kang, Y. Haldorai, K. Giribabu, G.-W. Lee, Y.-C. Lee, M.S. Hyun, Y.-K. Han, C. Roh, Y.S. Huh, Synergistically strengthened 3D micro-scavenger cage adsorbent for selective removal of radioactive cesium, Scientific reports 6 (2016) 38384.

[31] C.-E. Tsai, C.-W. Lin, B.-J. Hwang, A novel crosslinking strategy for preparing poly(vinyl

alcohol)-based proton-conducting membranes with high sulfonation, Journal of Power Sources 195 (2010) 2166-2173.
[32] H. Bessbousse, T. Rhlalou, J.F. Verchère, L. Lebrun, Removal of heavy metal ions from aqueous solutions by filtration with a novel complexing membrane containing poly(ethyleneimine) in a poly(vinyl alcohol) matrix, Journal of Membrane Science 307 (2008) 249-259.
[33] E. Salehi, S.S. Madaeni, L. Rajabi, V. Vatanpour, A.A. Derakhshan, S. Zinadini, S. Ghorabi, H. Ahmadi Monfared, Novel chitosan/poly(vinyl) alcohol thin adsorptive membranes modified with amino functionalized multi-walled carbon nanotubes for Cu(II) removal from water: Preparation, characterization, adsorption kinetics and thermodynamics, Separation and Purification Technology 89 (2012) 309-319.
[34] Y.H.F. Al-qudah, G.A. Mahmoud, M.A. Abdel Khalek, Radiation crosslinked poly (vinyl alcohol)/acrylic acid copolymer for removal of heavy metal ions from aqueous solutions, Journal of Radiation Research and Applied Sciences 7 (2014) 135-145.
[35] L. Zhang, J.Y. Wei, X. Zhao, F.Z. Li, F. Jiang, M. Zhang, X.Z. Cheng, Competitive adsorption of strontium and cobalt onto tin antimonate, Chemical Engineering Journal 285 (2016) 679-689.
[36] N. Minoo, L. Tong, P.S. Mark, D. Liming, W. Xungai, Electrospun single-walled carbon nanotube/polyvinyl alcohol composite nanofibers: structure–property relationships, Nanotechnology 19 (2008) 305702.
[37] G.M. Geise, D.R. Paul, B.D. Freeman, Fundamental water and salt transport properties of polymeric materials, Progress in Polymer Science 39 (2014) 1-42.
[38] D. González-Rodríguez, A.P.H.J. Schenning, Hydrogen-bonded Supramolecular π-Functional Materials, Chemistry of Materials 23 (2011) 310-325.
[39] M.S. Boroglu, S.U. Celik, A. Bozkurt, I. Boz, The synthesis and characterization of anhydrous proton conducting membranes based on sulfonated poly(vinyl alcohol) and imidazole, Journal of Membrane Science 375 (2011) 157-164.
[40] F.C. Ding, S.J. Wang, M. Xiao, Y.Z. Meng, Cross-linked sulfonated poly(phathalazinone ether ketone)s for PEM fuel cell application as proton-exchange membrane, Journal of Power Sources 164 (2007) 488-495.
[41] J. Seuba, S. Deville, C. Guizard, A.J. Stevenson, Mechanical properties and failure

behavior of unidirectional porous ceramics, Scientific reports 6 (2016) 24326.
[42] F. Gode, E. Pehlivan, Removal of chromium(III) from aqueous solutions using Lewatit S 100: the effect of pH, time, metal concentration and temperature, Journal of hazardous materials 136 (2006) 330-337.
[43] E.K. Yetimoglu, M.V. Kahraman, O. Ercan, Z.S. Akdemir, N.K. Apohan, N-vinylpyrrolidone/acrylic acid/2-acrylamido-2-methylpropane sulfonic acid based hydrogels: Synthesis, characterization and their application in the removal of heavy metals, React. Funct. Polym. 67 (2007) 451-460.
[44] J.-P. Simonin, On the comparison of pseudo-first order and pseudo-second order rate laws in the modeling of adsorption kinetics, Chem. Eng. J. 300 (2016) 254-263.
[45] A.A. Kadam, J. Jang, D.S. Lee, Facile synthesis of pectin-stabilized magnetic graphene oxide Prussian blue nanocomposites for selective cesium removal from aqueous solution, Bioresource Technology 216 (2016) 391-398.
[46] A.K. Vipin, S. Ling, B. Fugetsu, Sodium cobalt hexacyanoferrate encapsulated in alginate vesicle with CNT for both cesium and strontium removal, Carbohydrate Polymers 111 (2014) 477-484.
[47] S.-Y. Kang, J.-U. Lee, S.-H. Moon, K.-W. Kim, Competitive adsorption characteristics of Co2+, Ni2+, and Cr3+ by IRN-77 cation exchange resin in synthesized wastewater, Chemosphere 56 (2004) 141-147.
[48] S. Baik, H. Zhang, Y.K. Kim, D. Harbottle, J.W. Lee, Enhanced adsorption capacity and selectivity towards strontium ions in aqueous systems by sulfonation of CO2 derived porous carbon, RSC Advances 7 (2017) 54546-54553.
[49] O.D. Bonner, L.L. Smith, A Selectivity Scale for Some Divalent Cations on Dowex 50, The Journal of Physical Chemistry 61 (1957) 326-329.
[50] Y. Xu, W. Hong, H. Bai, C. Li, G. Shi, Strong and ductile poly(vinyl alcohol)/graphene oxide composite films with a layered structure, Carbon 47 (2009) 3538-3543.
[51] P. Cakir, S. Inan, Y. Altas, Investigation of strontium and uranium sorption onto zirconium-antimony oxide/polyacrylonitrile (Zr-Sb oxide/PAN) composite using experimental design, Journal of Hazardous Materials 271 (2014) 108-119.
[52] Y. Park, Y.-C. Lee, W.S. Shin, S.-J. Choi, Removal of cobalt, strontium and cesium from radioactive laundry wastewater by ammonium molybdophosphate–polyacrylonitrile (AMP–

PAN), Chemical Engineering Journal 162 (2010) 685-695.
[53] L. Zhang, J. Wei, X. Zhao, F. Li, F. Jiang, M. Zhang, X. Cheng, Competitive adsorption of strontium and cobalt onto tin antimonate, Chemical Engineering Journal 285 (2016) 679-689.
[54] L. Zhang, J. Wei, X. Zhao, F. Li, F. Jiang, M. Zhang, Strontium(II) adsorption on Sb(III)/Sb2O5, Chemical Engineering Journal 267 (2015) 245-252.

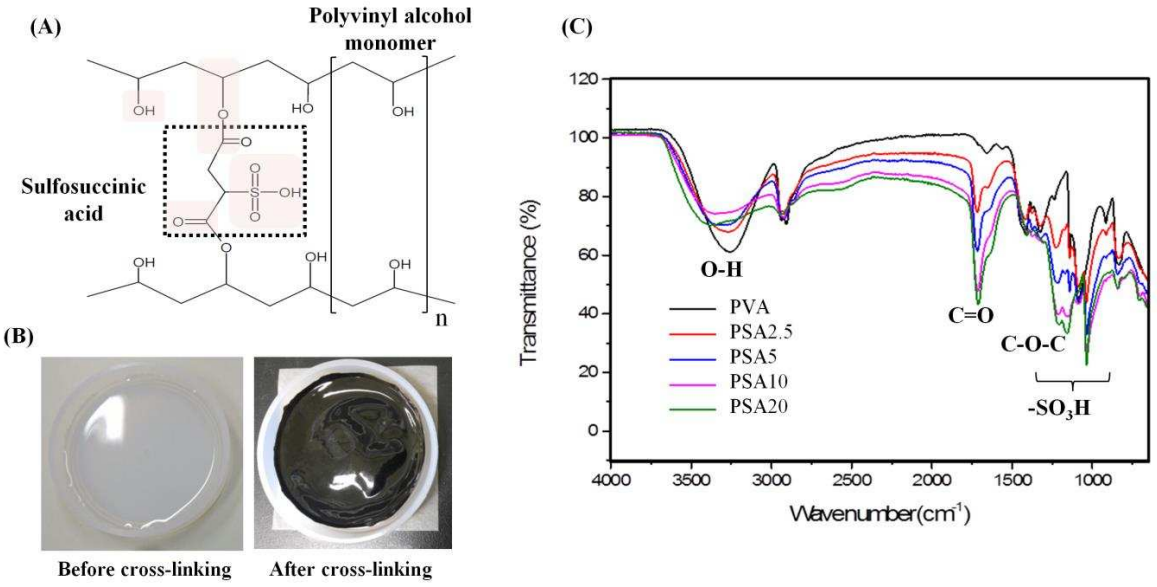

Figure 1. (A) Schematic of the chemical structure of polyvinyl alcohol (PVA) crosslinked with sulfosuccinic acid (SSA). (B) PVA membrane before and after crosslinking with SSA. (C) FT-IR spectra of PVA and PSA membranes.

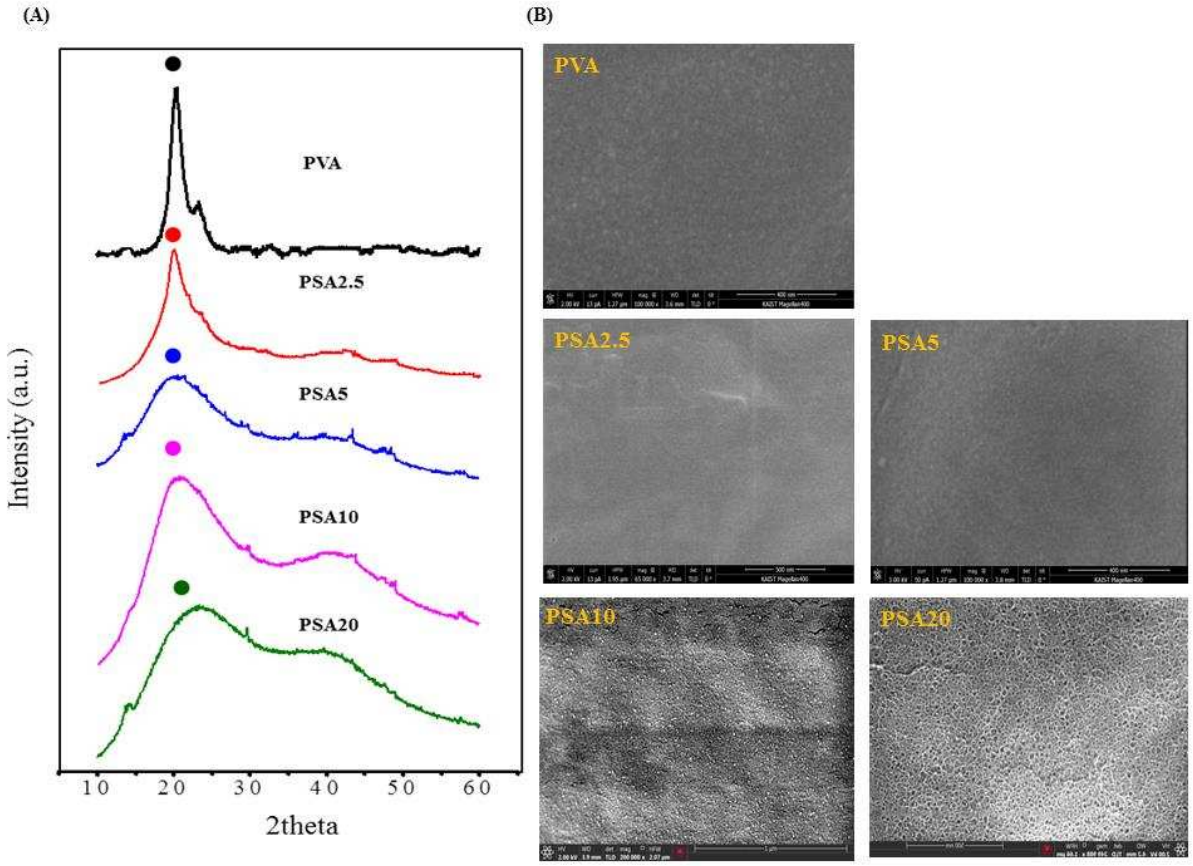

Figure 2. (A) X-ray diffraction patterns and (B) cryo-SEM images of PVA and PSA membranes.

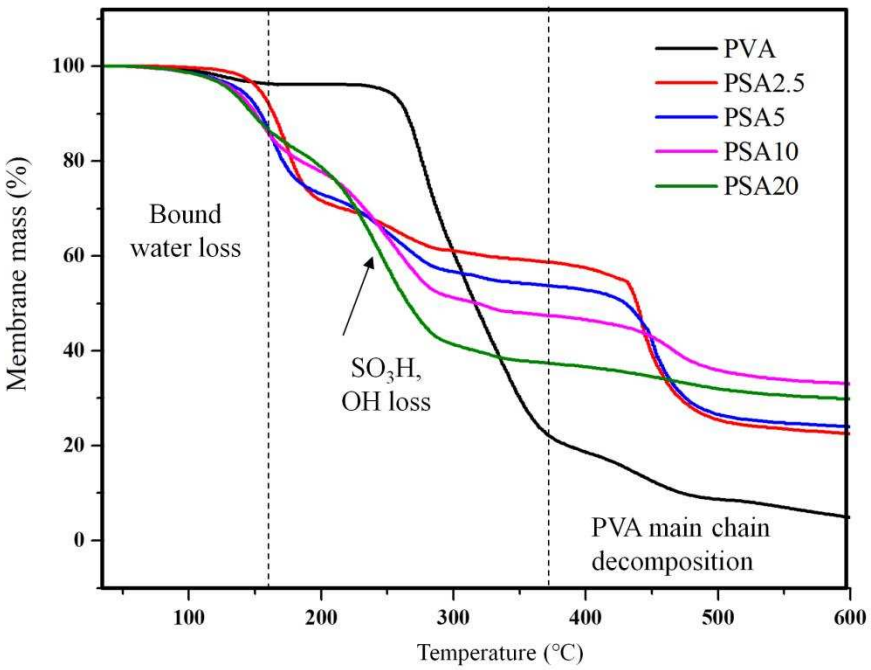

Figure 3. Thermogravimetric spectra of PVA and PSA membranes.

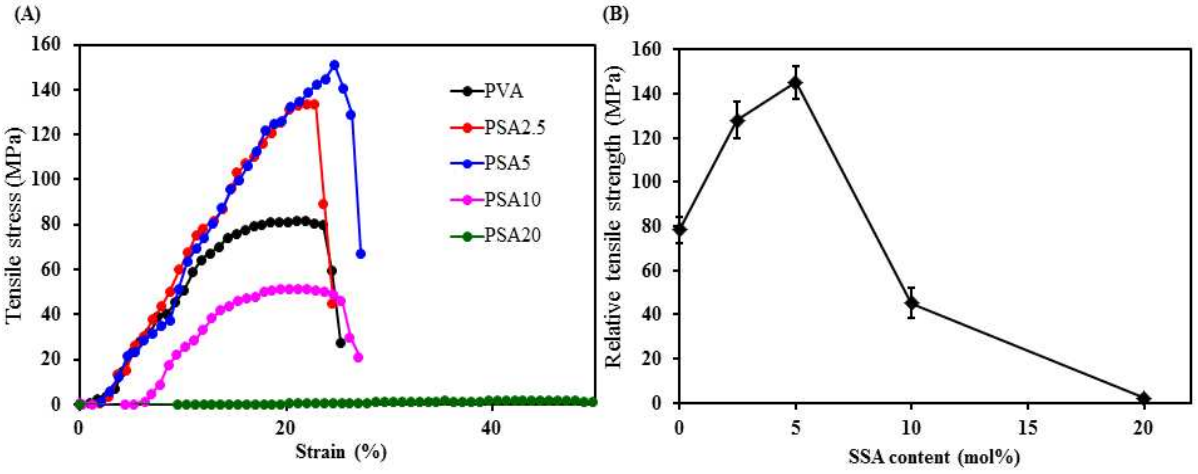

Figure 4. (A) Tensile stress (MPa) as a function of strain (%) for PVA and PSA membranes. (B) Maximum tensile stress (MPa) of PSA membranes of varying SSA content (mol%).

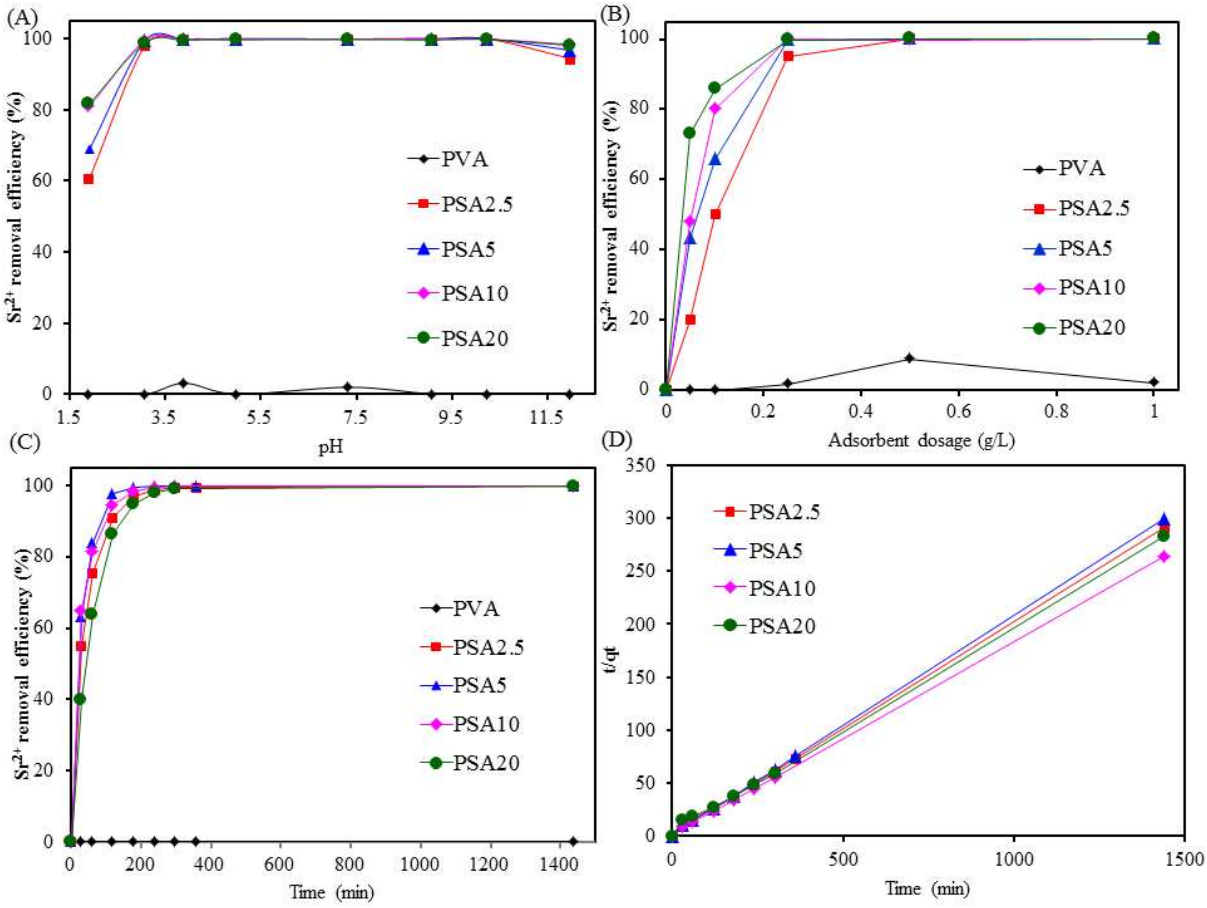

Figure 5. Effect of (A) pH, (B) adsorbent amount, (C) contact time for Sr^{2+} removal efficiency (%) by PVA and PSA membranes. (D) Pseudo-second order kinetic model for Sr^{2+} adsorption by PVA and PSA membranes. Initial Sr^{2+} concentration was 5 ppm in 20 mL simulated water, and the adsorbent concentration fixed at 1 g/L.

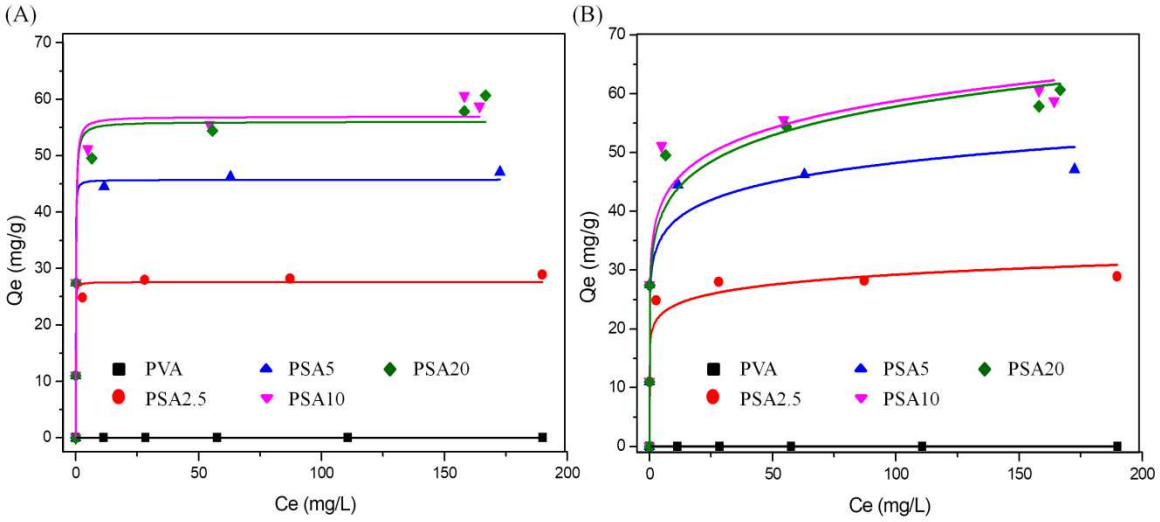

Figure 6. Sr^{2+} adsorption isotherms by PVA and PSA membranes fitted to (A) Langmuir and (B) Freundlich models.

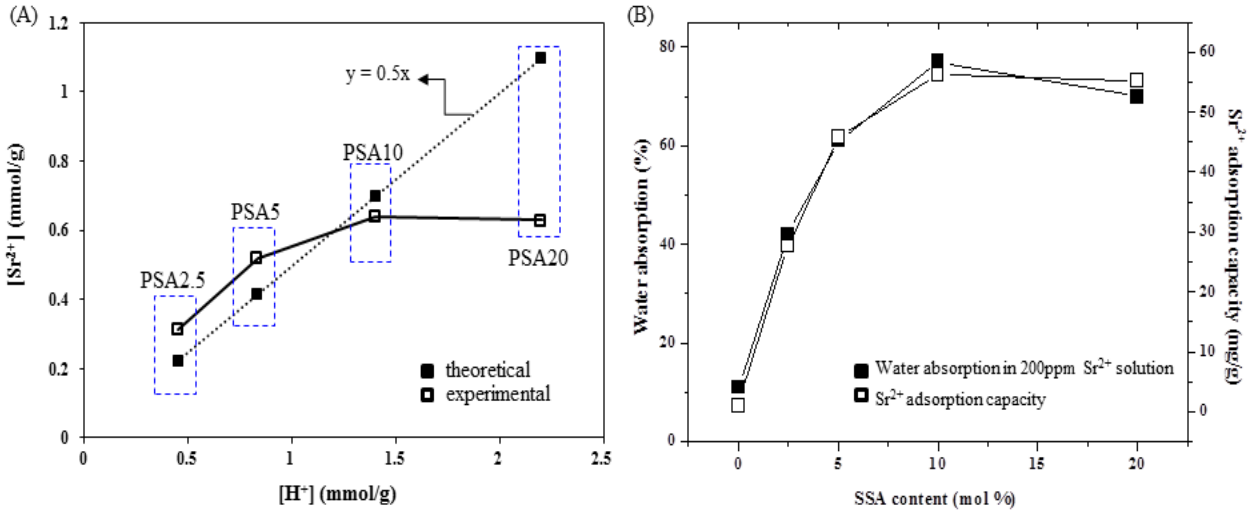

Figure 7. (A) A comparison of the experimental and theoretical Sr^{2+} exchange capacity of each PSA membrane in 200 ppm Sr^{2+} solution. (B) Water absorption (%) and Sr^{2+} adsorption capacity (mg/g) compared for all PSA membranes.

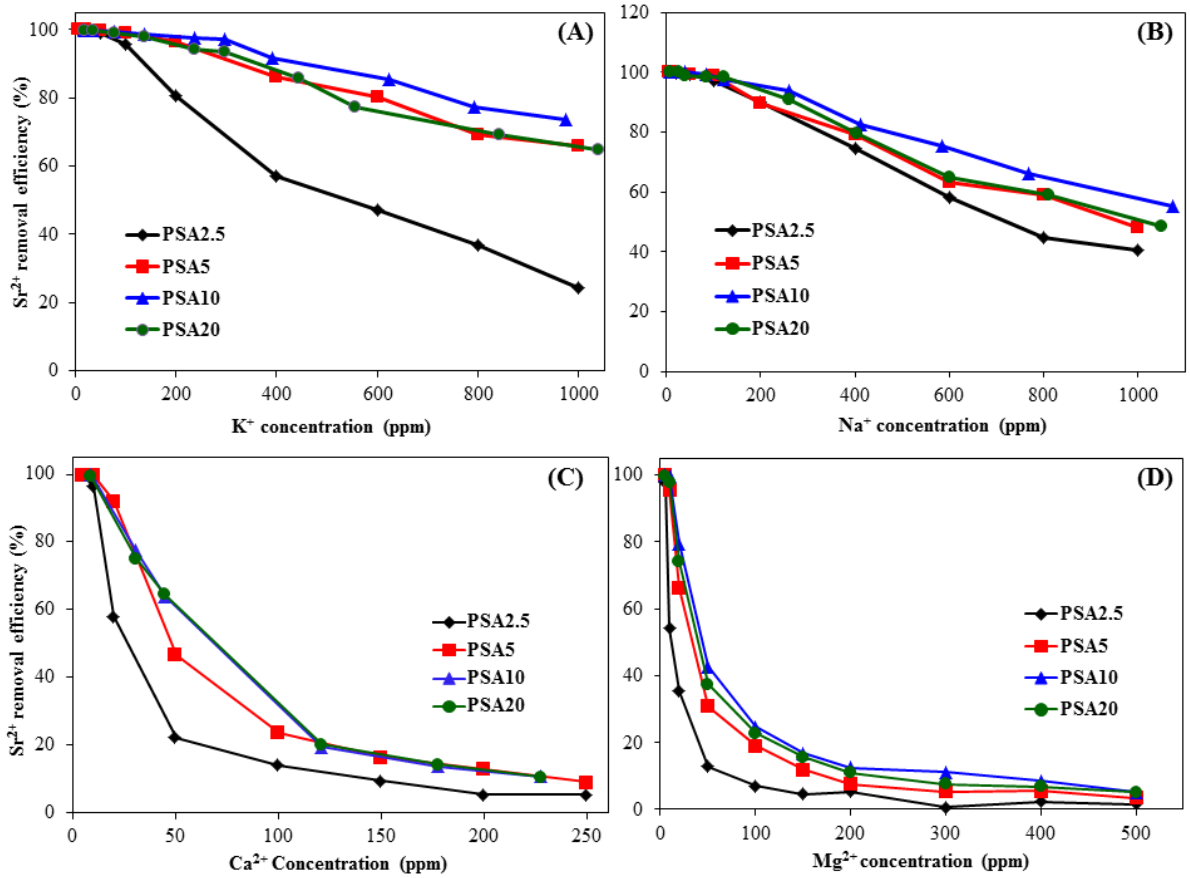

Figure 8. Effect of competitive ions and concentration on Sr^{2+} removal efficiency: (A) K^{+}, (B) Na^{+}, (C) Ca^{2+}, and (D) Mg^{2+}. The Sr^{2+} concentration was fixed at 5 ppm and the adsorbent amount equal to 1 g/L.

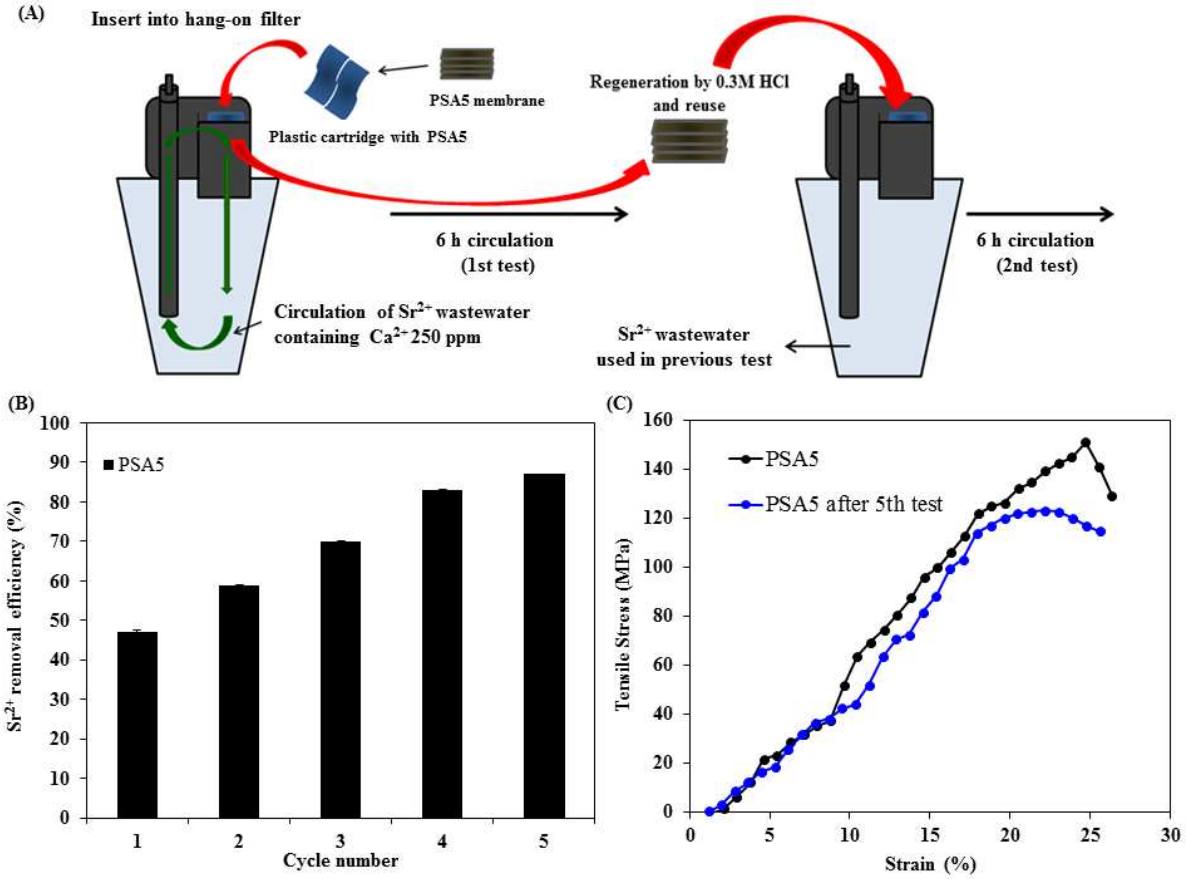

Figure 9. (A) Schematic of the membrane filtration setup for Sr^{2+} removal from simulated water containing 250 ppm Ca^{2+}. (B) Incremental increase in Sr^{2+} removal efficiency (%) by the PSA5 membrane mounted in the filtration cartridge (n.b. the initial (cycle 1) Sr^{2+} concentration equaled 5 ppm). (C) Tensile stress (MPa) as a function of strain (%) for PSA5 membranes prior to use and after 4 regeneration and 5 reuses.

Table 1. Mechanical properties of PSA and pure PVA membranes.

Sample	Tensile strength (MPa)	Young's modulus (MPa)	Elongation at break (%)
PVA	78.4 ± 6.2	363.4 ± 46.1	21.1
PSA2.5	128.1 ± 8.2	605.4 ± 4.6	22.8
PSA5	145.2 ± 7.5	622.3 ± 14.7	24.7
PSA10	45.2 ± 6.9	246.9 ± 51.9	21.2
PSA20	2.0 ± 0.3	5.0 ± 0.5	45.5

Table 2. Adsorption kinetic parameters for PSA membranes fitted using Pseudo-first order and Pseudo-second order model.

	Pseudo-first-order			Pseudo-second-order		
	Q_e (mg/g)	K_1(min^{-1})	R^2	Q_e (mg/g)	K_2 (min^{-1})	R^2
PSA2.5	4.95	0.0025	0.3941	5.00	0.08	0.9996
PSA5	4.80	0.0025	0.2919	4.82	0.05	0.9998
PSA10	5.47	0.0025	0.3762	5.50	0.04	0.9998
PSA20	5.09	0.0025	0.4499	5.17	0.14	0.9989

Table 3. Water absorption (%) by PVA and PSA membranes and associated Sr^{2+} adsorption parameters determined from Langmuir and Freundlich isotherm models.

	Water absorption (%)		Experimental value	Langmuir model			Freundlich model		
	Milli-Q water	Sr^{2+} 200 ppm solution	Qe^{*} (mg/g)	Q_m (mg/g)	b (L/mg)	R^2	K_f (mg/g)	n	R^2
PVA	10	9	0	0	0.957	-	0	1.90	-
PSA2.5	44	42	28.9	27.6	30.229	0.986	19.62	11.58	0.949
PSA5	65	61	47.1	45.8	25.311	0.986	30.29	9.91	0.926
PSA10	100	77	60.6	56.3	7.418	0.958	34.26	8.54	0.943
PSA20	177	70	60.7	55.3	7.224	0.977	32.10	7.83	0.940

Q_e^{*}: This vale is the maximum amount of Sr^{2+} adsorbed (mg/g) at equilibrium.

Table 4. Adsorption capacity of various Sr^{2+} adsorbents.

Adsorbents	Q_m (mg/g) of Sr^{2+}	Reference
Zr-Sb oxide/ poyacrylonitrile	43.67	[51]
Ammonium molybdophosphate-polyacrylonitrile	16.24	[52]
WO_3 coated Fe_3O_4	44.20	[2]
SnSb	22.9	[53]
$Sb(III)/Sb_2O_5$	25.7	[54]
Porous Carbon functionalized with SO_3H	18.97	[48]
PSA5	45.80	This work